NANO LETTERS

2008
Vol. 8, No. 4
1011-1015

Hyperfine Interactions in Graphene and Related Carbon Nanostructures

Oleg V. Yazyev†

Ecole Polytechnique Fédérale de Lausanne (EPFL), Institute of Chemical Sciences and Engineering (ISIC) and Institute of Theoretical Physics (ITP), CH-1015 Lausanne, Switzerland, and Institut Romand de Recherche Numérique en Physique des Matériaux (IRRMA), CH-1015 Lausanne, Switzerland

Received October 16, 2007; Revised Manuscript Received January 21, 2008

ABSTRACT

Hyperfine interactions, magnetic interactions between the spins of electrons and nuclei, in graphene and related carbon nanostructures are studied. By using a combination of accurate first principles calculations on graphene fragments and statistical analysis, I show that both isotropic and dipolar hyperfine interactions in sp^2 carbon nanostructures can be accurately described in terms of the local electron spin distribution and atomic structure. A complete set of parameters describing the hyperfine interactions of ^{13}C and other nuclear spins at substitution impurities and edge terminations is determined. These results permit the design of graphene-based nanostructures allowing for longer electron spin coherence times which are required by spintronics and quantum information processing applications. Practical recipes for minimizing hyperfine interactions in carbon nanostructures are given.

Graphene and related carbon nanostructures are considered as potential building blocks of future electronics, including spintronics[1] and quantum information processing based on electron spins[2] or nuclear spins. [3] Carbon nanostructures are attractive for these applications because of the weak spin–orbit interaction in materials made of light elements.[4,5] Very promising results for the spin-polarized current lifetimes in carbon nanotubes[6–9] and graphene[10,11] unambiguously confirm the potential of these materials. A number of quantum dot devices, components of solid-state quantum computers, based on carbon nanostructures have also been proposed recently.[12–16]

Hyperfine interactions (HFIs), the weak magnetic interactions between the spins of electrons and nuclei, become increasingly important on the nanoscale. In carbon nanostructures the interactions of electron spins with an ensemble of nuclear spins constitute the leading contribution to the electron spin decoherence.[4,7,17] Minimizing HFIs is thus necessary for achieving longer electron spin coherence times.[18] In some other instances the HFIs play an important role as a link between the spins of electrons and nuclei[3,19–21] in quantum information processing designs involving nuclear spins. Probing HFIs with magnetic resonance techniques also provides a wealth of information about structure and dynamics of carbon materials.[22] A common understanding and an ability to control the HFIs are thus necessary for engineering future-generation electronic devices based on graphene and related nanostructures.

In this Letter, I study the hyperfine interactions in carbon nanostructures by using a combination of accurate first principles calculations on graphene fragments and statistical analysis. I show that the interaction of the conduction (low-energy) π electron spins with nuclear spins can be described in terms of only the local (on-site and first-nearest-neighbor) π electron spin distribution and the local atomic structure. The conduction electron spin distribution can be determined using simpler computational approaches (e.g., tight binding or analytical approximations[23,24]) and tuned by tailoring nanostructure dimensions and applying external fields.[25,26] The local nature of HFIs justifies the extension of the obtained results from the nanometer scale to arbitrarily large nanostructures. I further extend my consideration to curved topologies and to the cases involving nuclear spins of other elements residing at impurities and boundaries.

The all-electron density functional theory (DFT) calculations were performed using the GAUSSIAN03 code.[27] A combination of the EPR-III Gaussian orbital basis set[28] specially tailored for the calculations of hyperfine couplings and the B3LYP exchange-correlation hybrid density functional[29,30] has been employed. This computational protocol (see ref 31 for details) can be applied to molecules of limited size and predicts hyperfine coupling constants (HFCCs) in excellent agreement with experimental results.[31] The present all-electron approach automatically accounts for exchange polarization of atomic core states.[32] Spin–orbit and relativistic effects which are not important for the calculation of HFIs in light-element systems[33] have not been taken into account. For a set of representative experimentally measured ^{13}C

† E-mail: oleg.yazyev@epfl.ch.

10.1021/nl072667q CCC: $40.75 © 2008 American Chemical Society
Published on Web 03/06/2008

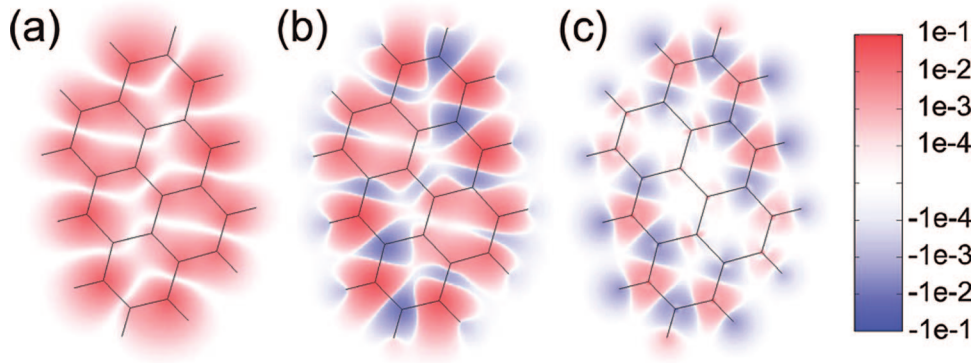

Figure 1. Projections of the spin-polarized conduction electron density $\rho_c^s(\mathbf{r})$ (a) and the total spin density ρ^s (**r**) (b) on the plane of an electron-doped graphene fragment (in au^{-2}). The total spin density ρ^s ($z = 0$) (c) in the plane of nuclei (in au^{-3}) reflects the isotropic hyperfine field. Molecular framework is shown by black lines.

isotropic HFCCs in graphenic ion-radicals,[34–36] the present computational methodology provides a mean absolute error of 1.1 MHz (≈2% of the range of magnitudes), which justifies the use of calculated HFCCs as a reference.

The effective spin-Hamiltonian of the HFI between the electron spin **S** and the nuclear spin **I** can be written as

$$\hat{\mathbf{H}} = \mathbf{S} \cdot \overleftrightarrow{\mathbf{A}} \cdot \mathbf{I}$$

where the 3 × 3 HFI tensor

$$\overleftrightarrow{\mathbf{A}} = A_{\mathrm{iso}} \cdot \overleftrightarrow{\mathbf{1}} + \overleftrightarrow{\mathbf{T}}$$

is usually decomposed into the scalar HFCC A_{iso} and the traceless dipolar HFI tensor $\overleftrightarrow{\mathbf{T}}$.[37] The HFI tensor $\overleftrightarrow{\mathbf{A}}$ reflects the distribution of the electron spin density $\rho^s(\mathbf{r}) = \rho^{\uparrow}(\mathbf{r}) - \rho^{\downarrow}(\mathbf{r})$ viewed from the position of the nucleus **I**. In carbon nanostructures the nuclear spins are those of the ^{13}C isotope (≈1.1% natural abundance and can be artificially changed; the dominant ^{12}C isotope has zero spin) and other elements originating from impurities and boundaries. The electron spin density $\rho^s(\mathbf{r})$ can further be decomposed into the contribution of half-populated conduction electron states lying close to the Fermi level (or singly occupied molecular orbitals in the molecular context)

$$\rho_c^s(\mathbf{r}) = \sum_c |\psi^c(\mathbf{r})|^2 \geq 0$$

and the contribution of the fully populated valence states perturbed by the exchange with spin-polarized conduction electrons[38]

$$\rho_v^s(\mathbf{r}) = \sum_v |\psi^{v\uparrow}(\mathbf{r})|^2 - |\psi^{v\downarrow}(\mathbf{r})|^2$$

The crucial role of this exchange-polarization effect is illustrated with a model electron-doped hydrogen-terminated graphene fragment in the doublet spin state (Figure 1). While the projection of $\rho_c^s(\mathbf{r})$ on the *xy* plane (Figure 1a) is positive every where and reveals an enhancement at the zigzag edges, the projection of the total spin-density $\rho^s(\mathbf{r})$ (Figure 1b) is negative where $\rho_c^s(\mathbf{r})$ is close to zero. The isotropic (Fermi contact) HFCC is proportional to the total spin density at the position of nucleus **I**,

$$A_{\mathrm{iso}} = \frac{4\pi}{3S} \beta_e \beta_N g_e g_I \rho^s(r_I)$$

where β_e and β_N are the Bohr and nuclear magnetons, while g_e and g_I are the g values of free electron and nucleus I, respectively.[37] S is the total spin. For the ideal graphene and planar sp^2 carbon nanostructures (all nuclei lie in the $z = 0$ plane) $\rho_c^s(z = 0) = 0$ due to the p_z symmetry of the conduction states. However, there is a contribution of the σ symmetry valence states $\rho_v^s(z = 0) \neq 0$ due to the exchange-polarization effect. For the model graphene fragment $\rho_v^s(z = 0)$ (Figure 1c) shows an alternating pattern with a relative dominance of the negative spin density. Since the σ states are situated well above and well below the Fermi level in sp^2 carbon nanostructures, the valence exchange-polarization phenomenon exhibits the property of locality. This property was exploited by Karplus and Fraenkel almost 50 years ago to describe the isotropic ^{13}C HFCCs in organic radicals.[39] The main contribution to the hyperfine anisotropy originates from the total spin population n of the on-site p_z atomic orbital, which also incorporates the contribution of exchange-polarized valence states. Assuming a local axial symmetry, $\overleftrightarrow{\mathbf{T}}$ can be written as a diagonal matrix with elements $T_{zz}/2 = -T_{xx} = -T_{yy} = A_{\mathrm{dip}}$, where

$$A_{\mathrm{dip}} = \frac{1}{5S} \beta_e \beta_N g_e g_I \langle r_{2p}^{-3} \rangle n$$

(r_{2p} is the distance of the carbon 2p electron to nucleus).

The HFIs were calculated for a set of 12 (~1 nm size) electron- and hole-doped planar hydrogen-terminated graphene fragments (Figure 2a) in the spin-doublet ground states. This provides a data set containing 206 inequivalent ^{13}C HFCCs. The calculated A_{iso} and A_{dip} values are fitted to the extended form of the Karplus–Fraenkel expression

$$A = a_j(1 + \sum_{i \in \mathrm{NN}} b_j \Delta r_i) n^c + c \sum_{i \in \mathrm{NN}} (1 + d\Delta r_i) n_i^c \qquad (1)$$

where the two terms account for the contributions of the on-site and nearest neighbor (NN) conduction electron spin populations per unpaired electron, n^c and n_i^c, respectively, calculated from first principles. The on-site coefficients a_j and b_j are distinguished for the cases of C atoms with three carbon NNs ($j = 3$) and the boundary atoms with two carbon

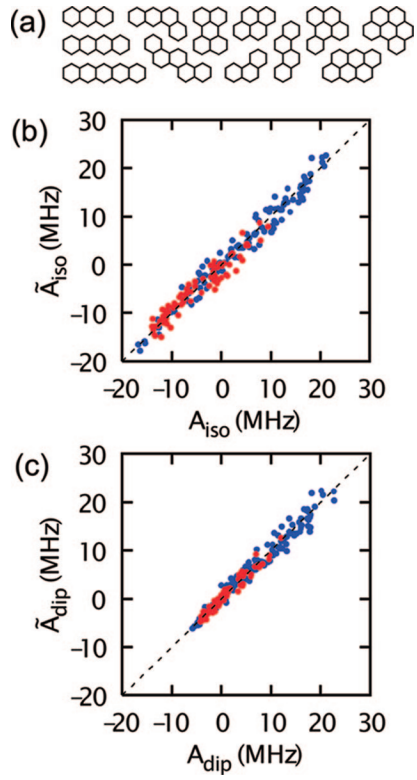

Figure 2. (a) Set of graphene fragments used in the present calculations. Predicted Fermi contact ($\tilde{A}_{iso}$) and dipolar ($\tilde{A}_{dip}$) ^{13}C HFCCs vs the corresponding values, A_{iso} (b) and A_{dip} (c), calculated from first principles. The values for inner (three carbon NNs) and boundary (two carbon NNs) atoms are shown as red and blue dots, respectively.

Table 1. Parameters (in MHz) Describing the HFIs of ^{13}C Nuclei in Graphene Fragments Obtained from the First Principles Calculations of a Set of Nanographite Molecules

	a_2	a_3	b_2	b_3	c	d
A_{iso}	162	128	2.3	6.1	−57.4	−7.4
A_{dip}	155	131	2.7	3.6	−19.4	−12.8

NNs ($j = 2$). The C−C bond length effects are encountered through the coefficients b_j and d with $\Delta r_i = r_i - r_0$ being the deviation of the bond length r_i from the value for the ideal graphene, $r_0 = 1.42$ Å. Only statistically significant local properties were included in the linear expression (1). The results of the regressions are summarized in Table 1(1 MHz = 4.136×10^{-3} μeV). Panels b and c of Figure 2 show the fitted (using eq 1 and regression parameters) values $\tilde{A}_{iso}$ ($\tilde{A}_{dip}$) versus the calculated A_{iso} (A_{dip}) values. Regressions to the linear expression (1) provide accurate estimations (root-mean-square errors are 1.7 and 1.2 MHz for A_{iso} and A_{dip}, respectively). The calculated isotropic HFCCs span about the same range of magnitudes (−16.7 MHz < A_{iso} < 21.1 MHz) as the dipolar HFCCs (−5.9 MHz < A_{dip} < 22.7 MHz). The HFCCs of boundary atoms tend to be larger due to the fact that low-energy states localize at the zigzag graphene edges.[23] The on-site and the NN exchange-polarization effects have competitive character ($a_3/c \approx -2$) in the case of isotropic HFCCs. The calculations predict ≈50% larger values for the parameters a_2, a_3, and c for A_{iso} compared to those obtained by Karplus and Fraenkel in their early studies of HFCCs in molecular radicals ($a_2 = 99.8$ MHz, $a_3 = 85.5$ MHz, and $c = -39$ MHz). [39] This difference

Table 2. Hyperfine Coupling Constants for Three General Cases of Spin Populations n^c on the Carbon Atoms in A and B Sublattices of Graphene

	$A_{iso}(A)/n^c$	$A_{iso}(B)/n^c$	$A_{dip}(A)/n^c$	$A_{dip}(B)/n^c$
$n^c_A = n^c_B > 0$	−44	−44	73	73
$n^c_A > 0$; $n^c_B = 0$	128	−172	131	−58
$n^c_A = -n^c_B > 0$	300	−300	189	−189

is probably due to the electron correlation effects incorporated (via DFT) in the calculations and due to the local atomic structure of the graphene lattice. Both A_{iso} and A_{dip} show a tendency to enhance the on-site and to weaken the NN contributions with the increase of C−C bond lengths. The dipolar HFCC is mostly influenced by the on-site contribution of the spin-polarized conduction state, and the NN exchange-polarization effect is weaker in this case ($a_3/c \approx -7$). When compared to typical solid state environments based on heavier elements, the ^{13}C HFCCs in graphene and related nanostructures are weaker and more anisotropic. For instance, a ^{31}P Fermi contact HFCC value of 117 MHz was found[40] for a shallow phosphorus donor in silicon crystal, Si:P, relevant to the solid-state quantum computing approach of Kane.[3,41] The difference is even more pronounced when carbon nanostructures are compared to GaAs often studied in the field of spintronics and quantum information processing. [41] In this material all natural isotopes (^{69}Ga, ^{71}Ga and ^{75}As) have spin 3/2, and HFIs dominate electron spin decoherence. The magnitudes of HFIs were estimated as $|A_{iso}/n^c| \sim 10^4$ MHz in this case.[41,42]

The graphene honeycomb lattice is a bipartite lattice, that is, it can be partitioned into two complementary sublattices A and B. I discuss the HFIs for the three general cases of conduction electron spin distributions over the sublattices: (i) ferromagnetic $n^c_A = n^c_B > 0$; (ii) ferrimagnetic $n^c_A > 0$ and $n_B{}^c = 0$; (iii) antiferromagnetic $n^c_A = -n^c_B > 0$ (cf. Table 2). The first case can be physically realized upon the uniform magnetization of the system with equivalent A and B sublattices, for example, by applying an external magnetic field. The negative $A_{iso} = -44$ MHz is small due to the partial compensation of the on-site and the NN exchange-polarization effects. This value is consistent with the values derived from the experimental ^{13}C Knight shifts in graphite intercalates[43] (−25 MHz < A_{iso} < −50 MHz) and with the calculated isotropic Knight shifts in metallic carbon nanotubes.[44] The ferrimagnetic case with the conduction state distributed over the atoms of only one sublattice (A) is physically realized at the zigzag edges[23] and around single-atom point defects in sublattice B.[45] Considerable alternating Fermi contact and dipolar HFCCs are predicted in this case. An antiferromagnetic pattern can be realized in the case of heavily disordered systems with localized defect and edge states in both sublattices.[46] The magnitudes of HFIs are minimized and maximized in the cases of ferromagnetic and antiferromagnetic electron spin distributions, respectively.

Many carbon nanostructures of reduced dimensionality (e.g., nanotubes and fullerenes) represent nonplanar topologies. Local curvatures lead to the sp^2-sp^3 rehybridization of carbon atoms and enable a Fermi contact interaction involving the low-energy π electron spins.[22] This results in a positive contribution of the π states unless n^c is close to zero; a contribution due to the NN exchange-polarization

Table 3. Parameters (in MHz) Describing the HFIs of Nuclei of Substitutional Impurities (^{11}B and ^{14}N), Monatomic Functional Groups (^{1}H and ^{19}F), and Rehybridized (sp^3) Carbon Atoms (^{13}C) at the Edges

		A_{iso}		A_{dip}	
nucleus	position	a	c	a	c
^{11}B	subst. impurity	43	−31	60	6
^{14}N	subst. impurity	150	−22	130	−10
^{1}H	C sp^2 edge	−119	22		
^{19}F	C sp^2 edge	240	−40		
^{1}H	C sp^3 edge		350		
^{19}F	C sp^3 edge		750		
^{13}C	C sp^3 edge		−68		

effect is negative in this case. The degree of rehybridization m of the π states (s^{m}p) can be described using a local bond angles analysis.[47] For the case of large curvature radii, the original expression for m can be reformulated in a more convenient form, $m = (d_{cc}^2/8)[1/R_1 + 1/R_2]^2$, where d_{cc} is the C−C distance, R_1 and R_2 are the principal curvature radii. The curvature-induced contribution to the Fermi contact ^{13}C HFCC is then

$$A_{iso}^{curv} = \frac{4\pi}{3S}\beta_e\beta_N g_e g_I nm\varphi_{2s}^2(0)$$

where $\varphi_{2s}(0)$ is the magnitude of the carbon atomic 2s wave function at the point of nucleus (for reference $8\pi/3\beta_e\beta_N 8 g_e g_I \varphi_{2s}^2(0) \approx 3.5\times10^3$ MHz). The curvature-induced direct coupling becomes significant ($m > 10^{-2}$) only in ultranarrow carbon nanotubes ($d < 1$ nm) and fullerenes.

Since the natural abundance of the "HFI-active" ^{13}C isotope is small (≈1%) and can be reduced further, the HFIs involving the nuclei of other elements can be significant or even dominant. Thus, their consideration is important for a complete description of HFIs in carbon nanostructures. The common substitution impurities in carbon are boron and nitrogen with all natural isotopes having nuclear spins. Graphene edges can be terminated by hydrogen[48] and fluorine atoms with both ^{1}H and ^{19}F spin-1/2 nuclei (99.9885% and 100% natural abundance, respectively) having high g values ($g(^1\text{H})/g(^{13}\text{C}) \approx g(^{19}\text{F})/g(^{13}\text{C}) \approx 4$). I consider HFIs in a reduced set of molecular fragments (only three- and four-ring structures included) with impurities and edge functionalizations in all possible positions. The calculated HFCCs have been fitted to the Karplus–Fraenkel relation, with no Δr terms included (Table 3). Both Fermi contact and dipolar HFCCs of the impurity nuclear spins show a monotonic increase along the ^{11}B−^{13}C−^{14}N series when compared to the results for ^{13}C HFCCs (Table 1). The NN relative-exchange-polarization effects (a/c ratio) on the Fermi contact HFCCs tend to decrease along the series. While the HFIs of the nuclear spins in substitution impurities are highly anisotropic, the hyperfine couplings of the edge nuclei show small anisotropy due to the sp^3 character of bonding. When ^{1}H and ^{19}F edge nuclei are bound to the sp^2 carbon atoms, the isotropic HFCCs are of the same order of magnitude as those of the ^{13}C spins in the graphene lattice. The influence of the NN carbon atoms (second NNs to the terminating atom) is very similar for ^{1}H and ^{19}F nuclei and smaller than in the case of ^{13}C HFCCs ($a_H/c_H \approx a_F/c_F \approx -6$). The spin polarization effect on ^{19}F HFCCs is stronger and of opposite sign compared to that of protons ($a_F/c_H \approx a_F/c_H \approx -2$). When edge atoms are bound to the rehybridized (sp^3) carbon atoms, n^c is zero but the NN contribution is significantly enhanced. The NN contribution to the ^{13}C hyperfine coupling of the sp^3 edge carbon atom itself ($c = -68$ MHz) has a similar magnitude as that of the sp^2 edge atoms ($c = -57$ MHz). HFIs with the boundary spins (H-terminated edges are often obtained in experiments[48]) have to be taken into account when designing carbon-based nanoscale devices for spintronics or quantum computing. A chemical modification of the graphene edges (e.g., substitution of the hydrogen atoms by alkyl-groups) can be suggested to reduce electron spin decoherence effects from the HFIs with boundary spins.

In conclusion, the results of first principles calculations show that the hyperfine interactions in graphene and related nanostructures are defined by the local distribution of the conduction electron spins and by the local atomic structure. Both Fermi contact and dipolar hyperfine interactions are about equally important in graphene-based nanostructures. Their magnitudes are significant, although in general smaller than the hyperfine couplings in materials based on heavier elements. A complete set of parameters describing the hyperfine interactions for the ^{13}C and other common nuclear spins was determined. This provides a tool for predicting the hyperfine interactions in sp^2 carbon nanostructures and permits control of these interactions by tailoring the chemical and isotopic compositions, local atomic structures, and strain fields. The present results can directly be applied to the design of graphene-based nanostructures optimal for spintronics and quantum information processing applications.

Acknowledgment. I acknowledge D. Loss and Yu. G. Semenov for motivating discussions, and S. Arey, D. Bulaev, L. Helm, V. G. Malkin, D. Stepanenko, and I. Tavernelli for comments on the manuscript. I also thank the Swiss NSF for financial support and CSCS Manno for computer time.

References

(1) Žutić, I.; Fabian, J.; Das Sarma, S. *Rev. Mod. Phys.* **2004**, *76*, 323.
(2) Loss, D.; DiVincenzo, D. P. *Phys. Rev. A* **1998**, *57*, 120.
(3) Kane, B. E. *Nature* **1998**, *393*, 133.
(4) Xiong, Z. H.; Wu, D.; Vardeny, Z. V.; Shi, J. *Nature* **2004**, *427*, 821.
(5) Bader, S. D. *Rev. Mod. Phys.* **2006**, *78*, 1.
(6) Tsukagoshi, K.; Alphenaar, B. W.; Ago, H. *Nature* **1999**, *401*, 572.
(7) Sahoo, S.; Kontos, T.; Schönenberger, C.; Sürgers, C. *Appl. Phys. Lett.* **2005**, *86*, 112109.
(8) Hueso, L. E.; Pruneda, J. M.; Ferrari, V.; Burnell, G.; Valdés-Herrera, J. P.; Simons, B. D.; Littlewood, P. B.; Artacho, E.; Fert, A.; Mathur, N. D. *Nature* **2007**, *445*, 410.
(9) Sahoo, S.; Kontos, T.; Furer, J.; Hoffmann, C.; Gräber, M.; Cottet, A.; Schönenberger, C. *Nat. Phys.* **2005**, *1*, 99.
(10) Hill, E. W.; Geim, A. K.; Novoselov, K.; Schedin, F.; Blake, P. *IEEE Trans. Magn.* **2006**, *42*, 2694.
(11) Tombros, N.; Jozsa, C.; Popinciuc, M.; Jonkman, H. T.; van Wees, B. J. *Nature* **2007**, *448*, 571.
(12) Bockrath, M.; Liang, W.; Bozovic, D.; Hafner, J. H.; Lieber, C. M.; Tinkham, M.; Park, H. *Science* **2001**, *291*, 283.
(13) Buitelaar, M. R.; Bachtold, A.; Nussbaumer, T.; Iqbal, M.; Schönenberger, C. *Phys. Rev. Lett.* **2002**, *88*, 156801.
(14) Trauzettel, B.; Bulaev, D. V.; Loss, D.; Burkard, G. *Nat. Phys.* **2007**, *3*, 192.
(15) Silvestrov, P. G.; Efetov, K. B. *Phys. Rev. Lett.* **2007**, *98*, 016802.
(16) Pereira, J. M.; Vasilopoulos, P.; Peeters, F. M. *Nano Lett.* **2007**, *7* (4), 946–949.
(17) Semenov, Y. G.; Kim, K. W.; Iafrate, G. J. *Phys. Rev. B* **2007**, *75*, 045429.

(18) Khaetskii, A. V.; Loss, D.; Glazman, L. *Phys. Rev. Lett.* **2002**, *88*, 186802.
(19) Taylor, J. M.; Marcus, C. M.; Lukin, M. D. *Phys. Rev. Lett.* **2003**, *90*, 206803.
(20) Epstein, R. J.; Mendoza, F. M.; Kato, Y. K.; Awschalom, D. D. *Nat. Phys.* **2005**, *1*, 94.
(21) Childress, L.; Dutt, M. V. G.; Taylor, J. M.; Zibrov, A. S.; Jelezko, F.; Wrachtrup, J.; Hemmer, P. R.; Lukin, M. D. *Science* **2006**, *314*, 281.
(22) Pennington, C. H.; Stenger, V. A. *Rev. Mod. Phys.* **1996**, *68* (3), 855.
(23) Nakada, K.; Fujita, M.; Dresselhaus, G.; Dresselhaus, M. S. *Phys. Rev. B* **1996**, *54*, 17954.
(24) Pereira, V. M.; Guinea, F.; Lopes dos Santos, J. M. B.; Peres, N. M. R.; Castro Neto, A. H. *Phys. Rev. Lett.* **2006**, *96*, 036801.
(25) Ţifrea, I.; Flatté, M. E. *Phys. Rev. Lett.* **2003**, *90*, 237601.
(26) Poggio, M.; Steeves, G. M.; Myers, R. C.; Kato, Y.; Gossard, A. C.; Awschalom, D. D. *Phys. Rev. Lett.* **2003**, *91*, 207602.
(27) Frisch, M. J.; Trucks, G. W.; Schlegel, H. B.; Scuseria, G. E.; Robb, M. A.; Cheeseman, J. R.; Montgomery, J. A.; Jr.; Kudin, K. N.; Burant, J. C.; Millam, J. M.; Iyengar, S. S.; Tomasi, J.; Barone, V.; Mennucci, B.; Cossi, M.; Scalmani, G.; Rega, N.; Petersson, G. A.; Nakatsuji, H.; Hada, M.; Ehara, M.; Toyota, K.; Fukuda, R.; Hasegawa, J.; Ishida, M.; Nakajima, T.; Honda, Y.; Kitao, O.; Nakai, H.; Klene, M.; Li, X.; Knox, J. E.; Hratchian, H. P.; Cross, J. B.; Adamo, C.; Jaramillo, J.; Gomperts, R.; Stratmann, R. E.; Yazyev, O.; Austin, A. J.; Cammi, R.; Pomelli, C.; Ochterski, J. W.; Ayala, P. Y.; Morokuma, K.; Voth, G. A.; Salvador, P.; Dannenberg, J. J.; Zakrzewski, V. G.; Dapprich, S.; Daniels, A. D.; Strain, M. C.; Farkas, O.; Malick, D. K.; Rabuck, A. D.; Raghavachari, K.; Foresman, J. B.; Ortiz, J. V.; Cui, Q.; Baboul, A. G.; Clifford, S.; Cioslowski, J.; Stefanov, B. B.; Liu, G.; Liashenko, A.; Piskorz, P.; Komaromi, I.; Martin, R. L.; Fox, D. J.; Keith, T.; Al-Laham, M. A.; Peng, C. Y.; Nanayakkara, A.; Challacombe, M.; Gill, P. M. W.; Johnson, B.; Chen, W.; Wong, M. W.; Gonzalez, C.; Pople, J. A. *Gaussian 03, Revision C.1*, Gaussian, Inc.: Wallingford, CT, 2004.
(28) Rega, N.; Cossi, M.; Barone, V. *J. Chem. Phys.* **1996**, *105*, 11060.
(29) Becke, A. D. *Phys. Rev. A* **1988**, *38* (6), 3098–3100.
(30) Becke, A. D. *J. Chem. Phys.* **1993**, *98* (7), 5648–5652.
(31) Hermosilla, L.; Calle, P.; García de la Vega, J. M.; Sieiro, C *J. Phys. Chem. A* **2005**, *109*, 1114.
(32) Yazyev, O. V.; Tavernelli, I.; Helm, L.; Röthlisberger, U. *Phys. Rev. B* **2005**, *71*, 115110.
(33) van Lenthe, E.; van der Avoird, A.; Wormer, P. E. S. *J. Chem. Phys.* **1998**, *108*, 4783.
(34) Bolton, J. R.; Fraenkel, G. K. *J. Chem. Phys.* **1964**, *40*, 3307.
(35) Fassaert, D. J. M.; de Boer, E. *Recl. Trav. Chim. Pays-Bas* **1972**, *91*, 273.
(36) Claridge, R. F.; Kirk, C. M.; Peake, B. M. *Aust. J. Chem.* **1973**, *26*, 2055.
(37) Kaupp, M.; Bühl, M.; Malkin, V. G., *Calculation of NMR and EPR Parameters: Theory and Applications.* Wiley-VCH: Weinheim, 2004.
(38) Goodings, D. A. *Phys. Rev.* **1961**, *123* (5), 1706.
(39) Karplus, M.; Fraenkel, G. K. *J. Chem. Phys.* **1961**, *35* (4), 1312.
(40) Overhof, H.; Gerstmann, U. *Phys. Rev. Lett.* **2004**, *92*, 087602.
(41) Schliemann, J.; Khaetskii, A.; Loss, D. *J. Phys.: Condens. Matter* **2003**, *15*, R1809.
(42) Paget, D.; Lampel, G.; Sapoval, B.; Safarov, V. I. *Phys. Rev. B* **1977**, *15*, 5780.
(43) Conard, J.; Estrade, H.; Lauginie, P.; Fuzellier, H.; Furdin, G.; Vasse, R. *Physica B* **1980**, *99*, 521–524.
(44) Yazyev, O. V.; Helm, L. *Phys. Rev. B* **2005**, *72*, 245416.
(45) Kelly, K.; Halas, N. *Surf. Sci.* **1998**, *416*, L1085.
(46) Yazyev, O. V.; Helm, L. *Phys. Rev. B* **2007**, *75*, 125408.
(47) Haddon, R. C. *J. Am. Chem. Soc.* **1986**, *108*, 2837–2842.
(48) Kobayashi, Y.; Fukui, K.-i.; Enoki, T.; Kusakabe, K. *Phys. Rev. B* **2006**, *73*, 125415.

NL072667Q